Contralateral Biases in Category-selective Areas Are Stronger in the Left Hemisphere than the Right Hemisphere

Sarah B. Herald[iD], **Hua Yang, and Brad Duchaine**

Abstract

■ Contralateral bias is a well-known feature of early visual cortex, but how it varies across higher-level, category-selective visual cortex and how much that bias differs between preferred and non-preferred is unclear. Here, we examined 12 category-selective regions across 4 experiments using peripherally presented faces, bodies, houses, and scenes, to measure the difference in contralateral bias between preferred and nonpreferred stimuli. The results showed a substantial range of contralateral biases across the category-selective regions, similar to prior studies using category-selective stimuli [Silson, E. H., Groen, I. I., & Baker, C. I. Direct comparison of contralateral bias and face/scene selectivity in human occipitotemporal cortex. *Brain Structure and Function, 227*, 1405–1421, 2022; Gomez, J., Natu, V., Jeska, B., Barnett, M., & Grill-Spector, K. Development differentially sculpts receptive fields across early and high-level human visual cortex. *Nature Communications, 9*, 788, 2018; Silson, E. H., Groen, I. I. A., Kravitz, D. J., & Baker, C. I. Evaluating the correspondence between face-, scene-, and object-selectivity and retinotopic organization within lateral occipitotemporal cortex. *Journal of Vision, 16*, 14, 2016; Kay, K. N., Weiner, K. S., & Grill-Spector, K. Attention reduces spatial uncertainty in human ventral temporal cortex. *Current Biology, 25*, 595–600, 2015; Silson, E. H., Chan, A. W.-Y., Reynolds, R. C., Kravitz, D. J., & Baker, C. I. A retinotopic basis for the division of high-level scene processing between lateral and ventral human occipitotemporal cortex. *Journal of Neuroscience, 35*, 11921–11935, 2015]. These contralateral biases were stronger in the left hemisphere regions than right, an asymmetry that was unchanged even when participants performed an attentionally demanding task. Thus, corresponding pairs of category-selective regions (e.g., left fusiform face area [lFFA] and right FFA [rFFA]) do not appear to be mirror images of each other; instead, the right hemisphere regions engage in greater integration of information from the two hemifields. The rFFA and right fusiform body area—both located on the right lateral fusiform gyrus—consistently had the weakest contralateral biases. That this asymmetry was most pronounced in the fusiform gyrus may account for why a unilateral lesion to the rFFA but not the lFFA can produce prosopagnosia. Together, our findings demonstrate that category-selective areas show pronounced differences in the extent of their contralateral biases and that a consistent asymmetry in the strength of the contralateral biases exists between the two hemispheres. ■

INTRODUCTION

In the earliest stages of cortical visual processing, visual input comes almost entirely from the contralateral visual field. In the later and more anterior stages, information from both the contralateral visual field and the ipsilateral visual field influence neural activity (Dumoulin & Wandell, 2008; Gross, 2008). Examining contralateral biases throughout visual cortex can provide insight into the functional organization of the visual system by revealing where and how information from the two visual fields is segregated and then integrated. Because early visual areas receive their initial input from the contralateral visual field, reduced contralateral bias in an ROI indicates that visual information transfer has occurred between the hemispheres either at the ROI or at prior regions along the visual hierarchy. fMRI is a powerful tool for studying contralateral biases because population-level contralateral biases can be measured in a substantial number of category-selective regions simultaneously.

Two approaches have been used in fMRI studies of contralateral biases in category-selective areas. The population receptive field (pRF) method displays stimuli at positions across the visual field and then models the BOLD responses of individual voxels to these stimuli to infer the size and position of pRFs. pRFs in areas selective for places, faces, and words have all been shown to be positioned primarily within a single contralateral visual field quadrant or hemifield, with a small but variable degree of spread outside the quadrant or hemifield (Finzi et al., 2021; Gomez, Natu, Jeska, Barnett, & Grill-Spector, 2018; Silson, Groen, Kravitz, & Baker, 2016; Silson, Chan, Reynolds, Kravitz, & Baker, 2015; Sayres & Grill-Spector, 2008). In the other method, visual stimuli are presented one at a time to the left and right visual fields (LVF and RVF, respectively) and the scaled difference in the BOLD signal between the two visual positions is calculated and used as the measure of contralateral bias. Because estimating contralateral biases does not require a pRF map of the

Dartmouth College

entire visual field, this alternate method provides a straightforward means to measure how contralateral biases are modulated by the stimulus presented. Hemond, Kanwisher, and Op de Beeck (2007) used this approach to measure the BOLD response to face, object, scene, or Fourier-scrambled images presented in either the LVF or RVF. They found strong contralateral bias in a combined V1 and V2 region as expected, but weaker and varied levels of contralateral bias in category-selective areas. Rauschecker, Bowen, Parvizi, and Wandell (2012) performed a similar study looking at the responses to words in the left and right visual word form area. In both left and right visual word form area, the response to words presented in the contralateral VF was twice the response of words presented in the ipsilateral VF, with no difference in the ratio between the hemispheres. Most recently, Pitcher et al. (2020) found that the right occipital face area (rOFA), right fusiform face area (rFFA), and left fusiform face area (lFFA) responded about 2–3 times more strongly to face videos in the contralateral versus the ipsilateral visual field whereas the face-selective regions in the right and left posterior superior temporal sulcus (pSTS) exhibited no contralateral bias.

We report contralateral bias estimates from six category-selective regions in each hemisphere. Here, we took a novel approach to calculating contralateral biases by making two modifications to the approach used in Hemond et al. (2007). First, we presented stimuli to both visual fields simultaneously. The simultaneous display of stimuli to both visual fields better simulates natural vision, where stimuli are present in both visual hemifields (Chelazzi, Duncan, Miller, & Desimone, 1998). We compared contralateral biases using this bilateral display to those found for unilateral displays in Experiment 3, and found that although this approach resulted in stronger estimates of contralateral biases across all ROIs compared with unilateral display methods, the relative degree of contralateral biases in each ROI was highly similar across both display methods. Second, we used the response to the bilateral nonpreferred stimuli (e.g., bilateral houses in FFA) as our baseline rather than a standard rest condition where

no stimulus is presented. This approach of contrasting responses to preferred and nonpreferred stimuli allowed us to measure contralateral biases in a manner similar to how these regions are localized. For example, our method examines the contralateral bias in FFA's response to faces versus houses rather than checkerboards or objects or even faces alone. Thus, our estimates of contralateral biases reflect how the category-selective signal changes between the LVF and RVF, unlike prior studies that may reflect the contralateral biases of the general visual response. Our results were robust across four experiments, showing similar estimates of contralateral biases to previous studies that examined a more limited set of ROIs (Gomez et al., 2018; Silson et al., 2015, 2016; Rauschecker et al., 2012; Hemond et al., 2007; Figure 1).

METHODS

Participants

Thirteen participants were scanned for Experiment 1 (sex unknown), 10 for Experiment 2 (five men), 11 for Experiment 3 (four men), and 10 for Experiment 4 (four men). We do not know the sex of the participants in Experiment 1 because we only have anonymized data. Our sample sizes were in line with previous studies of contralateral biases using similar methods (nine participants in Hemond et al., 2007; seven participants in Rauschecker et al., 2012). All participants were members of the Department of Psychological and Brain Sciences at Dartmouth College. Participants provided written informed consent, and all procedures were approved by Dartmouth's Committee for the Protection of Human Subjects.

Scanning Parameters

Experiment 1

Participants were scanned on a 3T Phillips MR scanner (Philips Medical Systems) using a SENSE (SENSitivity Encoding) 32-channel head coil. At the start of the scan, an anatomical volume was acquired using a high-resolution 3-D magnetization prepared rapid gradient

Figure 1. Four separate experiments were run, with Experiments 3 and 4 having two variations each. Experiments 1, 2, and 3 used black-and-white images whereas Experiment 4 used color images. In each experiment, participants fixated on the stimulus in the middle of the screen throughout the run.
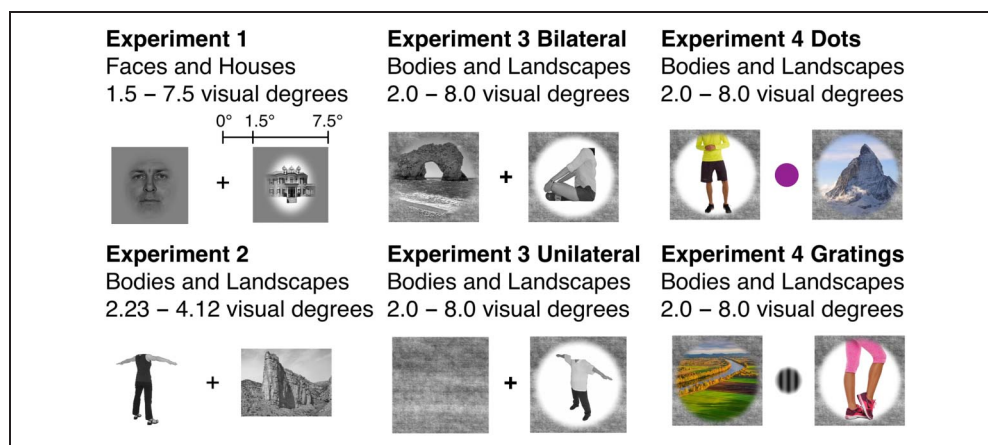
echo sequence (220 slices, field of view = 240 mm, acquisition matrix = 256 × 256, voxel size = 1 × 0.94 × 0.94 mm). Functional images were collected using echo-planar functional images (time to repeat = 2000 msec, time echo = 35 msec, flip angle = 90°, voxel size = 3 × 3 × 3 mm). Each volume consisted of 36 interleaved 3-mm thick slices with 0-mm interslice gap. The slice volume was set to cover most of the brain including the entire temporal lobe.

Experiments 2, 3, and 4

All functional and structural images were acquired using a 3T Siemens Magnetom Prisma MRI scanner (Siemens) with a 32-channel phased-array head coil. At the beginning of each scanning session, a T1-weighted structural scan was acquired using a high-resolution single-shot magnetization prepared rapid gradient echo sequence with an in-plane acceleration factor of 2 using generalized autocalibrating partially parallel acquisitions (GRAPPA): repetition time/echo time/inversion time = 2300/2.32/933 msec, flip angle = 8°, resolution = 0.9375 × 0.9375 × 0.9 mm voxels, matrix size = 256 × 256, field of view = 240 × 240 × 172.8 mm, 192 sagittal slices, ascending acquisition, anterior–posterior phase encoding, no fat suppression. Functional, BOLD images were acquired in an interleaved fashion using gradient-echo EPI with prescan normalization, fat suppression, a multiband (i.e., simultaneous multislice) acceleration factor of 4 (using blipped controlled aliasing in parallel imaging results in higher acceleration (CAIPIRINHA); Setsompop et al., 2012), and no in-plane acceleration (i.e., GRAPPA acceleration factor of 1): repetition time/echo time = 1000/35 msec, flip angle = 90° for Experiment 1 and 58° for Experiments 2, 3, and 4, resolution = 3 mm^3 isotropic voxels, matrix size = 96 × 96, field of view = 240 × 240 mm, 52 axial slices with full brain coverage and no gap, anterior–posterior phase encoding. At the beginning of each run, three dummy volumes were acquired to allow for signal stabilization. DICOM files were converted to NIFTI files using *dcm2niix* (Li, Morgan, Ashburner, Smith, & Rorden, 2016).

fMRI Tasks

For all fMRI tasks, MATLAB (Mathworks) and the Psycho-physics Toolbox Version 3 (Kleiner, Brainard, & Pelli, 2007; Brainard, 1997; Pelli, 1997) were used to display the stimuli and collect participant responses.

Functional Localizer

For Experiments 2, 3, and 4, each participant was scanned during five runs of a dynamic localizer. For the dynamic localizer, videos of faces, bodies, scenes, objects, and phase-scrambled objects were presented in a block design (Pitcher, Dilks, Saxe, Triantafyllou, & Kanwisher, 2011; Fox, Iaria, & Barton, 2009). Each block was 12 sec. For

Experiment 2, there was a 12-sec rest block in between each block. For Experiments 3 and 4, there was a 12-sec rest block at the beginning, middle, and end. Individual video clips were shown for 1.5 sec followed by a 0.5-sec blank ISI. Each stimulus category was shown once in the first half of the run and again in the second half of the run. During the first half of the run and again during the second half of the run, one of the video clips was played twice in a row. These blocks had the same length as the other blocks but had one less unique video stimulus because of the repeat. To maintain attention, participants were asked to press a button whenever a repeat occurred, but they were not told the frequency at which repetitions would occur. Except for these two attention checks, the video clips used within a run were never repeated. Subsequent runs of the localizer used the same video clips, although the block order was pseudorandomized for a balanced presentation order. Participants were allowed to freely view the stimuli throughout the run.

Contralateral Bias

Stimuli were presented simultaneously in the LVF and RVF, with the exception of a unilateral presentation condition in Experiment 3. For Experiment 1, faces and houses were used as the stimuli whereas bodies and landscapes were used for Experiments 2, 3, and 4.

Experiment 1

Each participant was scanned during three runs of the contralateral bias experiment. Black-and-white images of faces and houses were cropped in the same oval shape with a Gaussian blur applied to the edges. These cropped images were then overlaid on top of a square gray background to create the final image. The square images spanned 1.5–7.5 visual degrees from fixation in each visual field and were presented for 300 msec followed by a 200-msec blank ISI. Twenty images were presented in each block for a total block length of 10 sec. Blocks of bilateral faces, faces in the left and houses in the right VF, houses in the left and faces in the right VF, and bilateral houses were each presented 4 times. A 10-sec fixation block, which had no stimuli apart from a fixation cross, was interleaved between each stimulus block for a total run time of 5.5 m. Participants were told to fixate on a central cross throughout the run.

Experiment 2

To examine a different set of category-selective ROIs, the next experiment used images of bodies and landscapes to examine body- and scene-selective regions. Each participant was scanned during six runs of the contralateral bias experiment. Black-and-white images of bodies and landscapes were presented spanning 2.23–4.12 visual degrees from fixation in each visual field and were presented for 300 msec followed by a 200-msec blank ISI. Block

consisting of either bilateral bodies, bodies in the left and scenes in the right VF, scenes in the left and bodies in the right VF, and bilateral scenes were each presented 4 times for 10 sec with 10-sec rest blocks at the beginning, end, and between each block. The duration of a single run was 5.5 min. Participants were asked to fixate on a central cross throughout the runs. Four times during each run, a green dot was presented in the center of the image in either the LVF or RVF. Participants were asked to press a button whenever they noticed the green dot appear.

Experiment 3

To determine whether the presentation of bilateral stimuli produces results comparable to unilateral presentation, we ran a third experiment that included both unilateral and bilateral presentation conditions. Each participant was scanned with eight runs of the contralateral bias experiment. Black-and-white images of bodies and landscapes were presented bilaterally in the LVF and RVF as well as unilaterally in the LVF and RVF. Each image was cropped into a circular image with a Gaussian blur applied to the edges. These images were then overlaid on top of a square gray noise background created by phase-scrambling one of the images. The same noise background was used for each image. The square images spanned 2.0–8.0 visual degrees from fixation in each visual field and were jittered randomly 0.4 visual degrees horizontally and vertically when presented. Each image was presented for 300 msec followed by a 200-msec blank ISI. Blocks of bilateral bodies, bodies in the left and scenes in the right VF, scenes in the left and bodies in the right VF, bilateral scenes, bodies in the left VF, scenes in the left VF, bodies in the right VF, and scenes in the right VF were each presented 4 times for 10 sec with 10-sec rest blocks at the beginning and end. The duration of a single run was 5 min and 40 sec. Participants were asked to fixate on a central cross throughout the run. Eight times during the run, a green dot was presented in the center of the image on either the LVF or RVF. Participants were asked to press a button whenever they noticed the green dot appear.

Experiment 4

Results from Experiments 1, 2, and 3 showed hemispheric asymmetries in face-, body-, and scene-selective regions using both bilateral and unilateral presentations. Because hemispheric asymmetries have also been found in the attentional neglect literature (Nachev & Husain, 2006), we next examined whether attention was contributing to our observed hemispheric asymmetries. We moved attention away from the peripheral stimuli and manipulated the degree of attentional load. Unlike Experiments 1, 2, and 3, the attention task for this experiment was at fixation and targets appeared at a much higher frequency throughout the run to keep attention focused on a centrally positioned stimulus. Two tasks with differing attentional loads were

used to assess whether there was a relationship between attention and contralateral bias. The less attentionally demand task involved colored dots (Experiment 4 Easy), and the more attentionally demanding task involved black-and-white-oriented Gabor gratings (Experiment 4 Difficult).

Each participant was scanned during eight runs of the contralateral bias experiment, with all four easy task runs before the four difficult task runs. Color images of bodies and landscapes were cropped into a circular image with a Gaussian blur applied to the edges. Each image was then overlaid on top of a square gray noise background created by phase-scrambling one of the images. The same noise background was used for each image. The square images spanned 2.0–8.0 visual degrees from fixation in each visual field and were jittered randomly 0.4 visual degrees horizontally and vertically when presented. Each image was presented for 1800 msec followed by a 200-msec blank ISI. Blocks of bilateral bodies, bodies in the left and scenes in the right VF, scenes in the left and bodies in the right VF, and bilateral scenes were each presented 8 times for 6 sec. Six-second rest blocks occurred at the beginning of the run and after each block with visual stimuli. The total run time was 6 min and 36 sec.

Participants were asked to fixate throughout the run on a central, circular stimulus that spanned 1.0 visual degree at fixation. For the easy task runs, this stimulus was a colored dot that was presented for 100 msec followed by a 100-msec blank ISI. The dot changed color on each presentation. Participants were asked to press a button whenever a black dot appeared. For the difficult task runs, the stimulus was a Gabor patch that was presented for 100 msec followed by a 100-msec blank ISI. The Gabor patch changed orientation on each presentation. Participants were asked to press a button whenever the lines of the Gabor were oriented horizontally. Although the targets for both tasks only appeared for 100 msec, any button push within 1 sec of the target appearing was counted as correct. Before the start of each run, participants were shown the target (i.e., horizontal Gabor or black dot) and asked to push a button whenever the target appeared.

fMRI Analysis

For Experiments 1, 2, 3, and 4, surface-based segmentation and alignment was performed in FreeSurfer (https://surfer.nmr.mgh.harvard.edu/) using the *recon-all* command. Each participant's T1 scan, as well as a T2 scan if available, was used for surface reconstruction. The resulting FreeSurfer files were then prepared for analysis with AFNI (Analysis of Functional NeuroImages; Cox & Hyde, 1997; Cox, 1996) and SUMA (SUrface models and MApping; Saad & Reynolds, 2012; Saad, Reynolds, Argall, Japee, & Cox, 2004) using the *@SUMA_Make_FS* command to create standard surface meshes (Argall, Saad, & Beauchamp, 2006). AFNI's *afni_proc.py* (Taylor et al., 2018) command was used for analysis of the contralateral bias tasks. For Experiments 2, 3, and 4,

functional ROIs were selected by hand from standard anatomical locations using an independent dynamic localizer with a *t*-statistic threshold of at least 2.58 (*p* < .01, uncorrected). ROIs had to contain at least 10 contiguous voxels. For the face-selective regions, we looked for FFA near the lateral fusiform gyrus (Weiner, 2019) and for OFA near the inferior occipital gyrus (Gauthier et al., 2000). For body-selective regions, we looked for the fusiform body area (FBA) near the fusiform gyrus (Peelen & Downing, 2005) and for extrastriate body area (EBA) near the lateral occipito-temporal area (Downing, Jiang, Shuman, & Kanwisher, 2001). For scene-selective regions, we looked for parahippocampal place area (PPA) near the medial fusiform gyrus (Weiner, 2019) and for the occipital place area (OPA) near the transverse occipital sulcus (Dilks, Julian, Paunov, & Kanwisher, 2013). Because some participants had very large category-selective areas that spanned beyond the typical anatomical boundaries of the ROI and seemingly connected to different ROIs, we sometimes raised the *t*-statistic threshold to isolate the ROI. The maximum *t* value used was 4 for Experiment 2, 5 for Experiment 3, and 2.58 for Experiment 4. Some category-selective ROIs could not be localized in some participants because there were no category-selective voxels meeting the minimum *t*-statistic and cluster size thresholds near the standard anatomical locations for the ROI. The number of participants for whom each category-selective ROI could be localized in each experiment is shown in the results figures as "*n* = " in the data plot subtitle. Body-selective regions were localized using a contrast of bodies versus objects, and scene-selective regions were localized using a contrast of scenes versus objects.

Because an independent localizer was not available for Experiment 1, one of the task runs was used to localize face- and scene-selective regions. Voxels for the FFA and the PPA were selected from the corresponding cytoarchitectonic ROIs from Rosenke et al. (2018). FFA was confined to FG2 and FG4, and PPA was confined to FG1 and FG3. A separate hand-drawn region that did not overlap with FG1, FG2, FG3, or FG4 was created for OFA. The location of OFA for each participant and each localizer run was manually verified to be contained entirely inside the hand-drawn mask. The top 50 voxels with the highest *t* statistic for the bilateral faces minus bilateral houses (for FFA and OFA) or bilateral houses minus bilateral faces (for PPA) comparison were selected. The remaining two task runs were used to independently calculate the response to face and house stimuli in each visual field. This localization and testing was performed 3 times, each time leaving out a different task run as the independent localizer, with the responses to the two main task runs averaged across the three combinations.

For Experiments 1, 2, 3, and 4, a univariate surface-based analysis was performed with AFNI's *3dmaskave* for each participant using the selected functional ROIs. Two participants were excluded from Experiment 1 because their ROIs showed reverse selectivity in the hemifield task (e.g., face areas responded more to houses than

faces), suggesting a possible coding error in the timing files that cannot be fixed. Statistical analyses and data plotting were done using R (https://www.R-project.org), RStudio (https://www.rstudio.com), and the tidyverse package (Wickham et al., 2019).

Contralateral Bias Index

To quantify the degree of contralateral bias in each region, we created a contralateral bias index (CBI) for dual stimulus presentations. The index takes the following form: (Contralateral Preferred − Ipsilateral Preferred) ÷ (Contralateral Preferred − Bilateral Nonpreferred). For example, the index would be calculated in the right FFA (see Figure 2) as (FH − HF) ÷ (FH − HH), where FH is a face in the LVF and a house in the RVF, HF is a house in the LVF and a face in the RVF, and HH is a house in the LVF and a house in the RVF. A value of 1 would indicate that right FFA shows an increased BOLD response only to a face in the contralateral visual field (i.e., contralateral preferred condition) and shows no increased response to a face in the ipsilateral visual field (i.e., ipsilateral preferred condition) over the baseline of bilateral houses (i.e., bilateral nonpreferred condition). A value of 0 indicates that a face in the contralateral and ipsilateral visual field generate an equal BOLD response, and thus, there is no contralateral bias. For the unilateral condition in Experiment 3, the index takes the following form: ((Contralateral Preferred − Contralateral Nonpreferred) − (Ipsilateral Preferred − Ipsilateral Nonpreferred)) ÷ (Contralateral Preferred − Contralateral Nonpreferred). The more traditional index of contra − ipsi / (contra + ipsi) has a correlation of 0.74 with our index values, and use of it would not change the conclusions of this article.

Bilateral Boost

In addition to quantifying the difference between an ipsilateral and contralateral preferred stimulus presentation, we also quantified the effect of presenting two preferred stimuli simultaneously. This index takes the following form: (Bilateral Preferred − Contralateral Preferred) ÷ (Bilateral Preferred − Bilateral Nonpreferred). For example, the index would be calculated in the right FFA (see Figure 2) as (FF − FH) ÷ (FF − HH). Higher values indicate a stronger boost of the BOLD signal to two preferred stimuli compared with one preferred stimulus being presented. A value of 1 would indicate that the category-selective response only occurs if a face is presented in both visual fields simultaneously (an unrealistic outcome). A value of 0 in FFA would indicate that as long as a face (preferred stimulus) is shown in the contralateral visual field, there is no additional increase in the category-selective BOLD response to showing another face in the ipsilateral visual field. We report the bilateral boost for each ROI because our experimental design allowed us to calculate it, but because the primary purpose of the experiments was to investigate contralateral biases, we focus on the CBI.
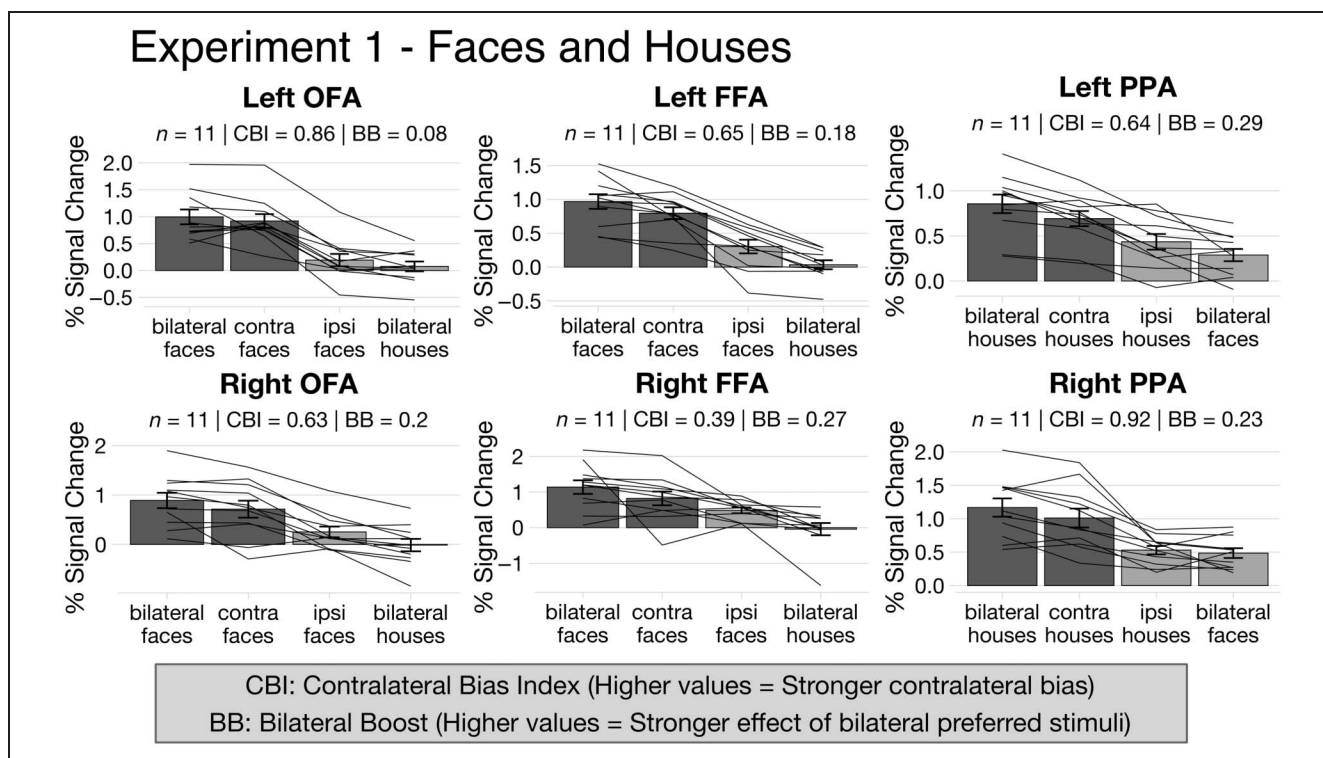
Experiment 1 - Faces and Houses

Figure 2. Results for Experiment 1. The y axis shows the beta value, which is equivalent to the percent signal change. The x axis shows the four conditions: bilateral pref (preferred stimuli in both visual fields), contra pref (preferred stimulus in the contralateral visual field and nonpreferred stimulus in the ipsilateral visual field), ipsi pref (preferred stimulus in the ipsilateral visual field and nonpreferred stimulus in the contralateral visual field), and bilateral non-pref (nonpreferred stimuli in both visual fields). For the face-selective regions (i.e., OFA and FFA), the preferred stimulus is faces and the nonpreferred stimulus is houses. For PPA, the preferred stimulus is houses and the nonpreferred stimulus is faces. The individual figure titles display the ROI name while the subtitle shows (from left to right), the number of participants for whom the ROI could be localized ("$n = $"), the CBI, and the bilateral boost (BB). The error bars show 1 *SEM*.

RESULTS

fMRI results are first presented for each individual experiment, followed by behavioral task performance and then a combined analysis of the fMRI data across all four experiments. Our results focus on the CBI, which combines data across the conditions and provides a straightforward quantification of the contralateral bias in each category-selective region. However, the group data for each condition as well as the individual participant data are displayed in the figures for each experiment.

Experiment 1

For Experiment 1, almost all the ROIs exhibited contralateral biases (Figure 2). A CBI value greater than 0.5 indicates that the region's category-selective response to the contralateral stimulus was at least twice as large as the category-selective response to the ipsilateral stimulus, which the CBI of the rOFA (0.63), lFFA (0.65), and the left parahippocampal place area (lPPA) (0.64) all exceeded. A value of 1 on the CBI indicates that the region only exhibits category-selectivity for contralateral stimulus, which both the rPPA and the lOFA came close to with CBI values of 0.92 and 0.86, respectively. The rFFA had the weakest contralateral bias, with a CBI of 0.39. Presenting the rFFA with

a face stimulus in the ipsilateral visual field (ipsilateral preferred condition) compared with two houses (bilateral nonpreferred condition) resulted in the largest increase in percent signal change between those two conditions among all the ROIs. The difference between those two conditions was greater than the difference found for moving the face stimulus from the ipsilateral visual field (ipsilateral preferred condition) to the contralateral visual field (contralateral preferred condition) for the rFFA. Finally, there was an asymmetry in the CBI of each ROI. Contralateral bias was greater in the left hemisphere for the OFA (left: 0.86; right: 0.63) and FFA (left: 0.65; right: 0.39) whereas it was greater in the right hemisphere for the PPA (left: 0.64; right: 0.92).

Experiment 2

In Experiment 2, we found that contralateral biases in category-selective regions extended beyond the face and place areas to the body areas as well, with all ROIs in Experiment 2 showing contralateral biases. The CBI for every ROI was greater in the left hemisphere than the right hemisphere. The rFBA had the lowest CBI (0.4). The FBA is located in the same region of cortex as the FFA, the lateral fusiform gyrus. Interestingly, the CBI for the rPPA (0.43) was similar to that of the rFBA (0.4).

The CBI in Experiment 2 of the lPPA (0.59) was greater than that of the rPPA (0.43) whereas the rPPA (CBI: 0.92) had a greater contralateral bias than the lPPA (CBI: 0.64) in Experiment 1. Because only the PPA was examined in both Experiments 1 and 2, it is unclear whether the variance in its CBI is because of the changes between the experiments or noise.

Experiment 3

Experiment 3 was similar to Experiment 2 but included a unilateral condition designed to test whether unilateral and bilateral presentations yield significantly different estimates of contralateral bias. The unilateral condition ($M = 0.38$, $SD = 0.18$) resulted in weaker estimates of contralateral biases for each ROI than the bilateral condition ($M = 0.59$, $SD = 0.14$), $t(7) = -10.039$, $p < .0001$, paired t test. This difference was almost entirely because of a comparable reduction in the contralateral biases across all regions in the unilateral condition as evidenced by the high correlation between the unilateral and bilateral CBI values, $r(6) = .96$, $p = .0002$, and the nearly identical downward left shifts of the data points in Figure 6C. Although our bilateral method finds stronger contralateral biases than the unilateral method, the ordering of the ROIs' CBIs is the same and the relative distances between the ROI CBIs are highly similar between both methods.

The CBIs for the lEBA and rEBA were almost identical in Experiments 2 and 3 (lEBA: 0.72 vs. 0.76; rEBA: 0.57 vs. 0.56). The lFBA and rFBA also had similar estimates in each experiment (lFBA: 0.5 vs. 0.6; rFBA: 0.4 vs. 0.3). The lPPA was highly similar between experiments (0.59 vs. 0.6).

However, the CBIs for the rPPA (0.43 vs. 0.62), lOPA (0.79 vs. 0.55), and rOPA (0.57 vs. 0.75) showed larger differences between experiments. Notably, these differences also meant that the hemispheric asymmetry between the PPA and OPA reversed, although the PPA's CBI values were very similar between hemispheres, suggesting little to no hemispheric asymmetry. Across the three experiments, the PPA had a stronger contralateral bias in the right hemisphere for Experiment 1, a stronger bias in the left hemisphere for Experiment 2, and no asymmetry for Experiment 3. There was no significant difference between the percentage of dots detected for the LVF ($M = 68\%$, $SD = 23\%$) versus the RVF ($M = 71\%$, $SD = 8\%$), $t(10) = -0.40159$, $p = .6964$, paired t test, indicating that participants attended to both visual fields to a similar degree.

Experiment 4

In the first three experiments, left hemisphere regions tended to show greater contralateral biases than right hemisphere regions. One possible explanation for this hemispheric asymmetry is that participants attended to the stimulus in the LVF more than the RVF. The increased attention to the LVF might then produce a corresponding increase in the BOLD response of the right hemisphere. If attention increased the BOLD signal equally for both stimulus categories (Reddy, Kanwisher, & VanRullen, 2009), then our method of subtracting the response to the nonpreferred category from the preferred category would cause the equivalent BOLD signal increases to cancel out. However, if attention selectively enhances the preferred category, then hemispheric asymmetries could arise. To directly address this attentional account, we ran
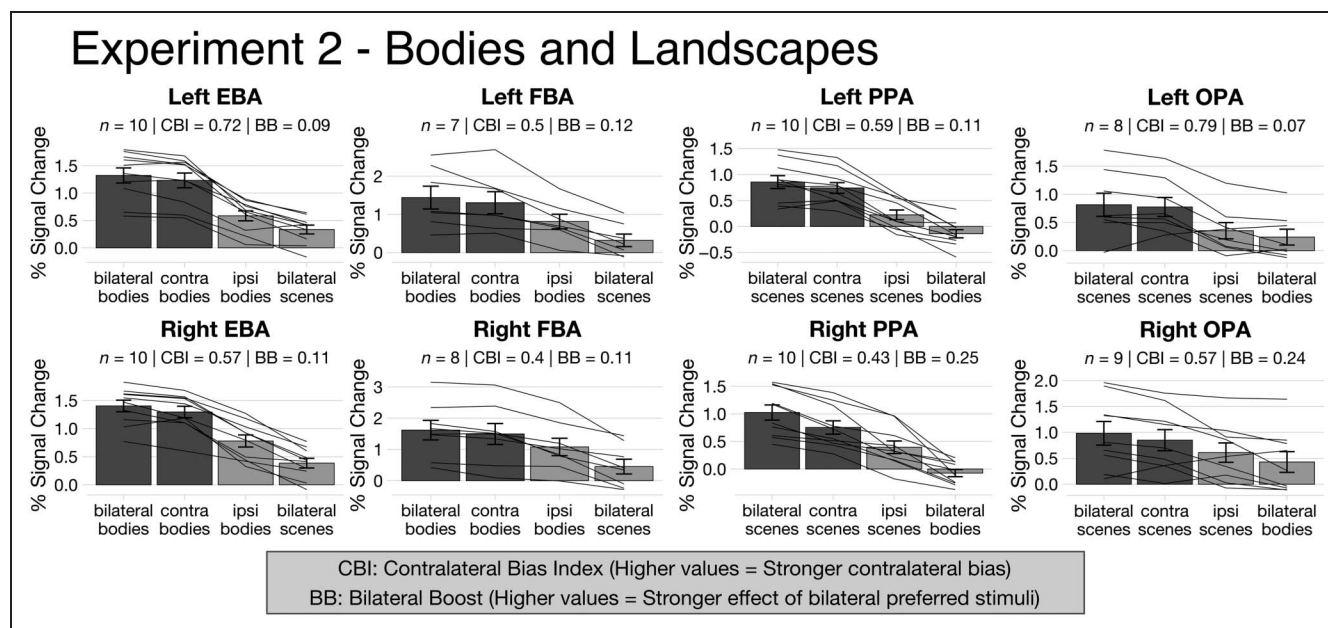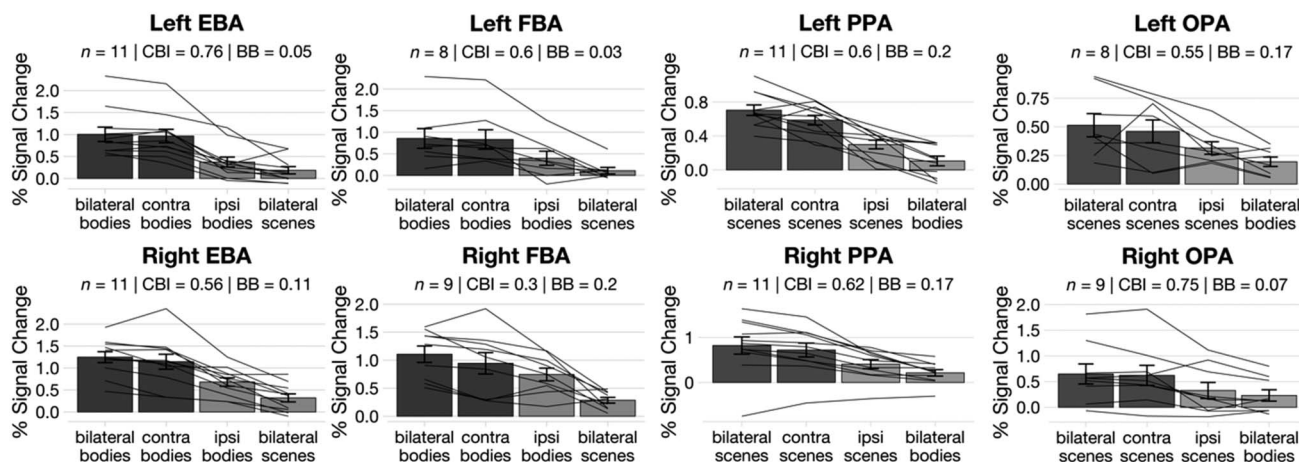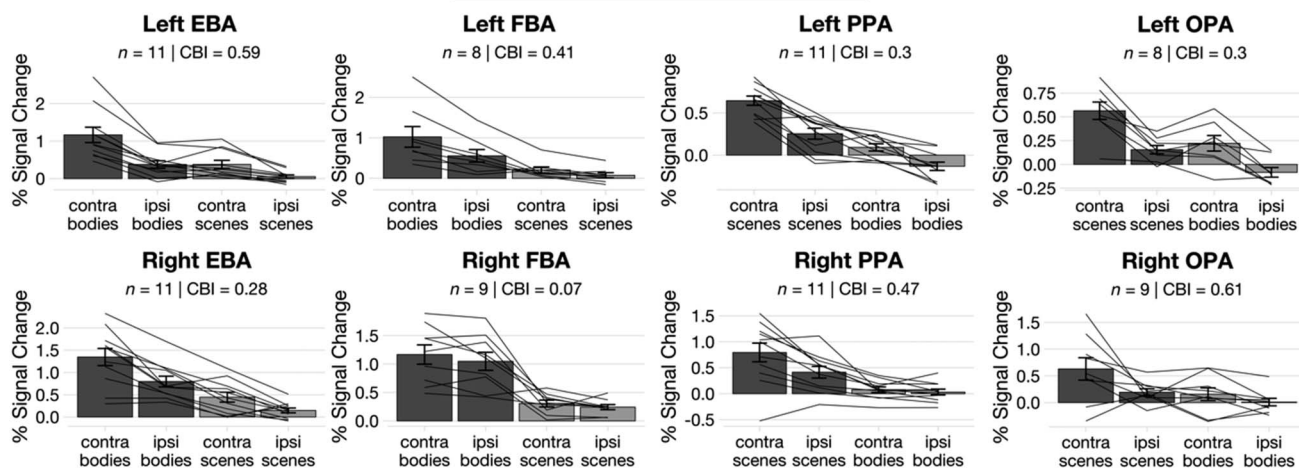

Figure 3. Results for Experiment 2. The layout of the bar plots is the same as Figure 2 except for the stimuli used. For the body-selective regions (i.e., EBA and FBA), the preferred stimulus is bodies and the nonpreferred stimulus is landscapes. For the scene-selective regions (i.e., PPA and OPA), the preferred stimulus is landscapes and the nonpreferred stimulus is bodies.

Figure 4. Results for Experiment 3. The individual plots are the same as Figure 2 except for the stimuli used. For the body-selective regions (i.e., EBA and FBA), the preferred stimulus is bodies and the nonpreferred stimulus is landscapes. For the scene-selective regions (i.e., PPA and OPA), the preferred stimulus is landscapes and the nonpreferred stimulus is bodies. The top two rows show the results from the bilateral presentation condition whereas the bottom two rows show the results unilateral presentation condition.

a fourth experiment in which participants performed two different, attentionally demanding tasks at fixation.

The effect of attention on CBIs was measured in a low-attention condition (Figure 5A) and a high-attention condition (Figure 5B). As expected, participants in Experiment 4 were significantly more accurate at detecting the target stimulus for the easy task ($M = 89\%$, $SD = 9\%$) than the difficult task ($M = 61\%$, $SD = 11\%$), $t(9) = 9.3715$, $p < .0001$, paired t test. Although the CBIs were lower in the easy task condition ($M = 0.55$, $SD = 0.20$) than the difficult condition ($M = 0.62$, $SD = 0.22$), this difference was not significant, $t(7) = -2.0585$, $p = .07853$, 95% CI [-0.1531, 0.0106], paired t test. Furthermore, there was a high

correlation between the CBIs for the easy and difficult task conditions, $r(6) = .89$, $p = .0027$, indicating that differences between the two conditions are largely attributable to a shift in contralateral biases that was comparable across all ROIs and not a change in the relative ranking of each ROI's contralateral bias. As a result, the greater contralateral biases in the left hemisphere than the right hemisphere do not appear to result from attentional factors.

The PPA and OPA showed greater contralateral biases in the left hemisphere than the right hemisphere for both attention conditions. The EBA had a higher CBI in the left hemisphere for the easy task condition, but almost no hemispheric asymmetry for the difficult task condition.

Finally, the FBA was again consistent with Experiments 2 and 3, with a higher CBI in the left hemisphere than the right hemisphere for both attention conditions as well as the rFBA having the lowest CBI of all the ROIs.

Combined Results: Contralateral Biases

Our data across Experiments 1, 2, 3, and 4 showed category-selective contralateral biases were present in each ROI ($M = 0.60$, $SD = 0.18$), $t(37) = 20.989$, $p < .0001$, 95% CI [0.54, 0.66], one-sample t test. These contralateral biases varied by ROI, and in some cases were quite strong (e.g., lEBA: $M = 0.77$, $SD = 0.08$). Indeed, only 9 out of 38 ROI CBIs (24%) were less than 0.5

(weaker contralateral bias) [rFBA (×4), rOPA (×2), rPPA (×2), rFFA], of which only rFBA and rFFA were below 0.5 each time they were measured (average CBI for rFFA: 0.39; average CBI for rFBA: 0.38). Figure 6B demonstrates this visually, with the CBIs for nearly all ROIs being clustered in the top half of the figure (right hemisphere CBI > 0.5) and many in the top right quadrant (left and right hemisphere CBI > 0.5).

Combined Results: Lateral Fusiform Gyrus

rFFA and rFBA showed weaker contralateral biases (lower CBIs) than lFFA and lFBA, respectively, across the four experiments. rFFA and rFBA also had the weakest
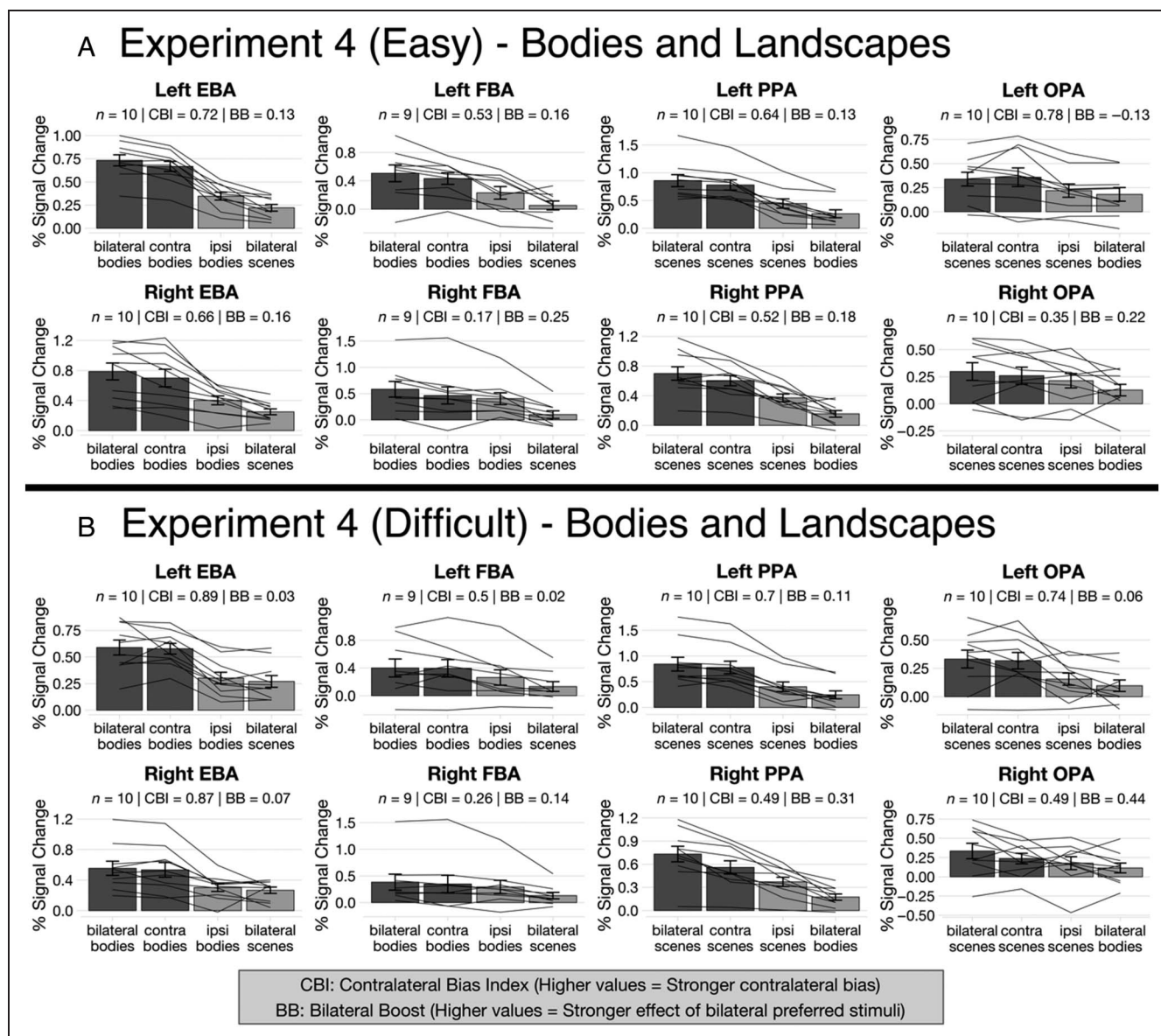

Figure 5. Results for Experiment 4. The layout of the bar pots is the same as Figure 2. Participants carried out one of two attentional tasks in each run. The easy task required detection of a black dot in a rapid stream of colored dots, and the difficult task required detection of horizontally oriented Gabors in a rapid stream of Gabors. The estimated contralateral bias for each region is similar across both tasks, and rFBA again has the weakest contralateral bias in both tasks. Thus, the hemispheric asymmetries observed in the contralateral bias estimates do not appear to result from hemispheric differences in attention.
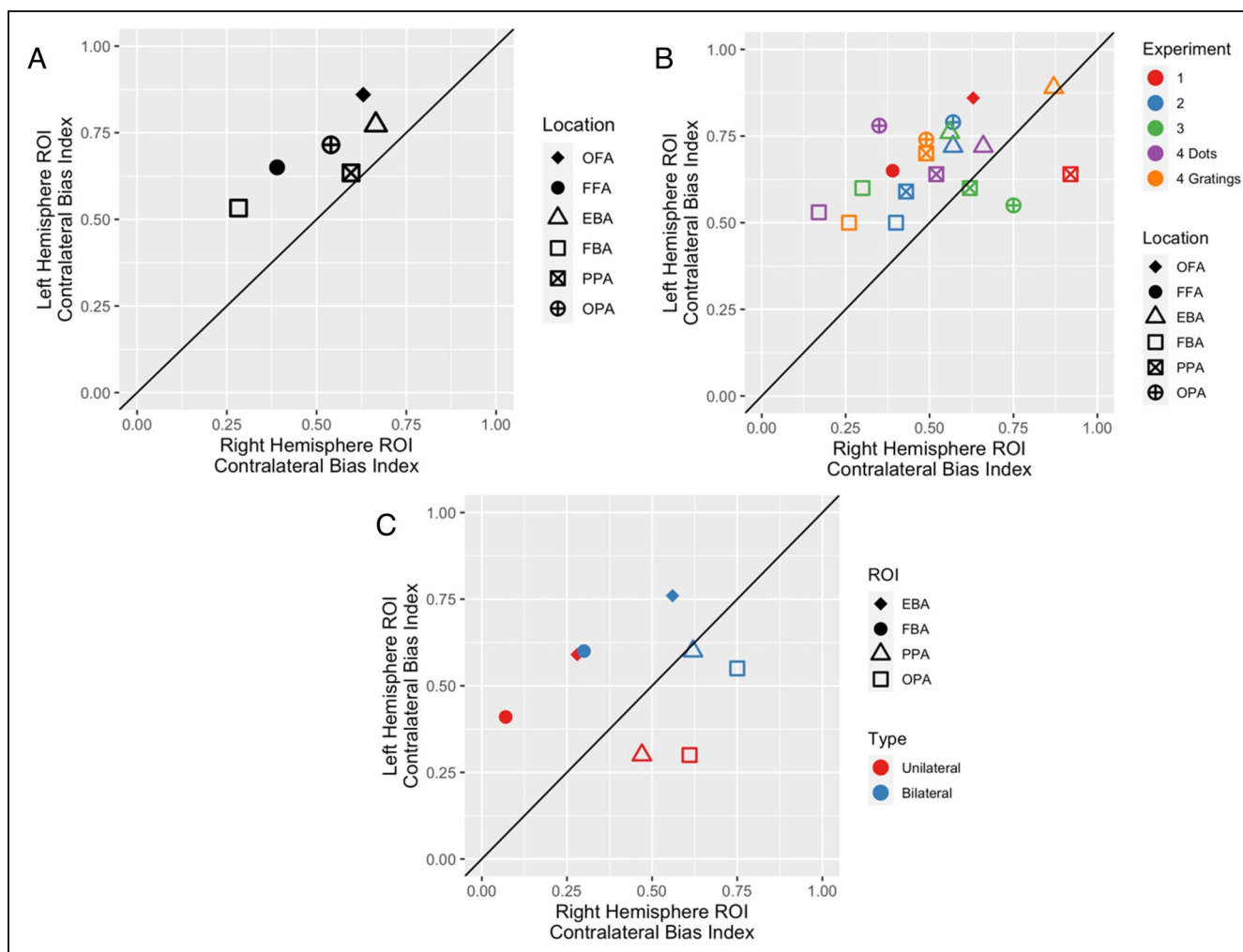
Figure 6. (A) To visualize the hemispheric asymmetry in contralateral biases across all four bilateral experiments, each category-selective region was averaged across all four experiments and plotted together. Data from the unilateral presentation condition of Experiment 3 are not included. Each point on the plot represents a category-selective region (e.g., FBA). The y axis shows the value of the CBI in the corresponding left hemisphere region (e.g., lFBA), whereas the x axis shows the CBI value in the right hemisphere (e.g., rFBA). Lower CBI values indicate more similar responses to stimuli in the contralateral and ipsilateral visual fields. Regions that lie above the line of equivalence have stronger contralateral bias in the left hemisphere than the right hemisphere. (B) Similar to A, each category-selective region has been plotted but with the individual data points from each experiment instead of averaging them across experiments. (C) To visualize the effect of unilateral versus bilateral presentations, the unilateral and bilateral data from Experiment 3 has been plotted on the same figure.

contralateral bias (lowest index values) of all ROIs for each experiment. Both ROIs are which can be seen are clustered on the left side of the scatterplot, demonstrating their weak contralateral bias in the right hemisphere (Figure 6B). For the Hemisphere × ROI ANOVA, Tukey's HSD test showed that the only significant differences for ROIs were between FBA and all other ROIs except FFA (FBA-EBA: $p < .001$, FBA-OPA: $p = .016$, FBA-PPA: $p = .017$, FBA-OFA: $p = .020$, EBA-FFA: $p = .348$, FFA-OFA: $p = .467$, PPA-EBA: $p = .498$, OPA-EBA: $p = .678$, PPA-OFA: $p = .748$, OPA-OFA: $p = .830$, FBA-FFA: $p = .853$, OPA-FFA: $p = .875$, PPA-FFA: $p = .915$, EBA-OFA: $p > .999$, OPA-PPA: $p > .999$).

Combined Results: Hemispheric Asymmetry

There was a clear asymmetry between the contralateral biases in left and right hemisphere ROIs. A two-way Type

I ANOVA with Hemisphere (i.e., left or right) and ROI (i.e., OFA, FFA, EBA, FBA, PPA, OPA) as factors revealed a significant main effect of Hemisphere, $F(1, 26) = 12.5642$, $p = .0015$, with the left hemisphere ($M = 0.67$, $SD = 0.12$) having higher index values than the right hemisphere ($M = 0.52$, $SD = 0.20$), and a significant main effect of ROI, $F(5, 26) = 6.2247$, $p = .0006$. There was no significant interaction between Hemisphere and ROI, $F(5, 26) = 0.8625$, $p = .5192$. The widespread asymmetry of contralateral bias can be seen in Figure 6. ROIs above the line of equivalence have a stronger average contralateral bias in the left than the right hemisphere.

DISCUSSION

In four experiments, we measured contralateral biases in six bilateral category-selective areas. This study offers

a broad examination of contralateral biases across category-selective cortex that allows comparisons between the strength of the biases for different category-selective areas. This bird's-eye approach revealed a striking hemispheric asymmetry in which contralateral biases were more pronounced in left hemisphere areas than right hemisphere areas, even after attention was controlled for. The contralateral biases across these areas also exhibited a substantial range, with two areas on the right lateral fusiform gyrus, the rFFA and rFBA, consistently having the weakest contralateral biases. Below, we discuss each of these findings, previous relevant results, and the implications for the organization of visual recognition.

Hemispheric Asymmetry and Hemispatial Neglect

The hemispheric asymmetry of contralateral biases echoes a fundamental asymmetry in neuropsychological disorders affecting visual attention. In hemispatial neglect, unilateral damage—typically to the parietal lobe or the temporal-parietal junction—results in stimuli in the contralateral visual field failing to reach awareness (Husain & Rorden, 2003; Driver & Vuilleumier, 2001). Hemispatial neglect is much more likely to persist in cases with a unilateral lesion to the right hemisphere than to the left hemisphere. This asymmetry is seen as evidence that the two hemispheres have differential access to information in the ipsilateral visual field: Right hemisphere attentional mechanisms have access to information from both visual fields whereas left hemisphere mechanisms have more limited access to ipsilateral information (Heilman & Van Den Abell, 1980). As a result, information from the RVF is still available to attentional mechanisms after a left hemisphere lesion, but information from the LVF is no longer available following damage to right hemisphere attentional processes (Driver & Mattingley, 1998).

Our results suggest that the differential access that attentional processes in the left and right hemisphere have to information from the ipsilateral visual field is mirrored by the asymmetric contralateral biases in category-selective areas. In both cases, information from the RVF is better represented in the right hemisphere than LVF information is in the left hemisphere. However, the hemispheric asymmetries we observed remained and were even strengthened in many regions when attentional load was increased away from the category stimuli. Thus, these regions appear to have fundamental hemispheric asymmetries in their contralateral biases that are not the result of attentional modulation. Because the participants in Experiment 4 showed undiminished contralateral biases when they attended to tasks at fixation, our study could be seen to tentatively suggest that the attentional asymmetry revealed by hemispatial neglect may be a downstream effect of asymmetries in the category-selective areas. If this account is correct, hemispheric asymmetries in category-selective areas in patients with hemispatial neglect may

be comparable to the asymmetries found in neurotypical participants.

Relation to Population-receptive Fields and Preferential Processing of Preferred Stimuli

One explanation for the hemispheric asymmetry in our results (Figure 6) is that they are a reflection of the rFFA and rFBA having more foveal pRFs than the lFFA and lFBA (Gomez et al., 2018). However, our stimuli were presented in the periphery with the inner edge at 2° of fixation. Assuming the lFFA and lFBA have more peripheral pRFs, they should have stronger levels of activation to the contralateral stimulus than their corresponding right hemisphere regions. However, the category-selective response to the contralateral preferred stimulus was nearly the same in the left and right FFA and FBA across all experiments. The decrease in contralateral bias in the right hemisphere is driven almost entirely by a substantially increased category-selective response to the ipsilateral preferred stimuli. It appears that information from the left FFA and FBA is transferred and integrated into the rFFA and rFBA in a gated manner so that it occurs for their preferred stimulus (i.e., faces or bodies) but does not occur for their nonpreferred stimuli (e.g., houses or checkerboards). It is this transfer of information that is asymmetrical, such that the right hemisphere either does not transfer information or only transfers a limited amount of information to the lFFA when viewing a face in the contralateral visual field.

Broad Contralateral Biases

There was a substantial range of contralateral biases found throughout category-selective cortex. In figures displaying results from the individual experiments (Figures 2–5), these biases can be seen in the greater response to preferred stimuli in the contralateral visual field than the ipsilateral visual field. Figure 6 presents summaries of the contralateral biases across the four experiments, with greater CBI values indicating greater contralateral biases.

A factor possibly contributing to the strength of the contralateral biases we observed is our bilateral stimulus paradigm, which we used because it better simulates natural vision than unilateral presentations. To compare the two methods, Experiment 3 contained both the bilateral stimulus paradigm as well as the previously used unilateral stimulus paradigm (Pitcher et al., 2020; Rauschecker et al., 2012; Hemond et al., 2007). The results from Experiment 3 revealed that contralateral biases were weaker when stimuli were presented unilaterally (average CBI across all ROIs: 0.38) than bilaterally (average CBI across all ROIs: 0.59). However, the relative amounts of contralateral bias in each ROI were not affected by the type of presentation as they were strongly correlated with each other ($r = .96$).

Hemispheric Asymmetry in Scene-selective Regions

Unlike the face- and body-selective areas, PPA and OPA did not exhibit the same direction of hemispheric asymmetry across all experiments. For both ROIs, CBI was greater in the left than right hemisphere in Experiments 2 and 4, but greater in the right than left for OPA and about equal for PPA in Experiment 3. In addition, PPA's CBI was greater in the right than the left hemisphere for Experiment 1. The large variance in PPA and OPA's hemispheric asymmetry suggests that there may be little or no hemispheric asymmetry and that any difference seen in the experiments is simply random variance around a zero mean. Indeed, when averaging across the Experiments in Figure 6A, PPA demonstrates almost no hemispheric asymmetry whereas OPA exhibits a slightly smaller degree of hemispheric asymmetry (as determined by the shortest distance from the data point to the line of equivalence).

Evidence for the degree of hemispheric asymmetry present in PPA is mixed. Silson et al. (2015) found little hemispheric asymmetry in PPA. In contrast, Uyar, Shomstein, Greenberg, and Behrmann (2016) found that rPPA had a greater degree of contralateral bias than lPPA, with lPPA exhibiting little to no contralateral bias. Silson et al. (2016) found a small degree of hemispheric asymmetry in OPA. It is possible that unlike EBA and FBA, PPA and OPA may have larger variance in the hemispheric asymmetry of their contralateral bias across individuals. Regardless, it seems clear that the consistency of measurements in EBA of FBA is much greater than that of PPA and OPA.

Ventral versus Dorsal ROIs

Silson, Groen, and Baker (2022) examined the relationship between the degree of selectivity in face- and scene-selectivity ROIs and the degree of contralateral bias. They found that ventral ROIs–FFA and PPA–exhibited stronger selectivity but weaker contralateral bias than the more dorsal ROIs–OFA and OPA. Given the inconsistent results in hemispheric asymmetry for the scene-selective ROIs across our four experiments, it is difficult to assess whether this relationship holds true for our study. Looking at the average CBI across all experiments (Figure 6A), OFA, PPA, OPA, and EBA all have a similar degree of contralateral bias in both hemispheres with no clear distinction between the ventral (PPA) and dorsal ROIs (OFA, OPA, EBA). FFA and FBA have the least contralateral bias for both hemispheres.

Strong Integration in Right Lateral Fusiform Gyrus and Unilateral Prosopagnosia

Because we looked at a large set of category-selective regions across multiple anatomical regions and separately within each hemisphere, we were able to observe the degree to which the rFFA and the rFBA stood as outliers. As seen in Figure 6, these ROIs reliably had the weakest contralateral biases. Although we chose to localize the

face-selectivity on or near the fusiform gyrus as one region (FFA), a face-selective region on the posterior fusiform (pFus) and another on the medial fusiform (mFus) can often be identified (Weiner et al., 2014). Uyar et al. (2016) examined contralateral bias in FFA1 (pFus) and FFA2 (mFus) and found stronger contralateral bias in the right hemisphere than left hemisphere for FFA1 but not FFA2. In contrast, Gomez et al. (2018) measured contralateral bias for pFus (FFA1) and found stronger contralateral bias in the left hemisphere than the right. We were not able to reliably localize pFus and mFus, making direct comparisons to our study difficult. However, stronger contralateral bias in right pFus than right mFus might suggest that the right ventral face selective regions initially contain a more contralaterally biased representation reflecting their early visual inputs before integrating visual information from the other hemisphere into a less contralaterally biased representation.

Our study cannot address the time course of the information transfer underlying this integration, but EEG studies of face processing suggest hemispheric asymmetries are not present with the initial information transfer across hemispheres and only emerge later. Towler and Eimer (2015) measured ERP responses to faces and houses using a simultaneous, bilateral display of faces and houses similar to the presentations used in our study. They found that the peak of the N170 in both hemispheres was influenced by visual information purely from the contralateral visual field. Because their study found no hemispheric asymmetries, it suggests that the asymmetry in our results only begins to emerge in later stages of processing. Ince et al. (2016) examined the N170 in more detail using the Bubbles technique and found that the initial part of the N170 was largely coding the contralateral eye while the later part of the N170 reflected information from the ipsilateral eye as well. The authors did not, however, find an asymmetry in the transfer of this information between the hemispheres. Thus, it appears the initial peak response, as measured by the N170, is solely from the contralateral visual field, that both hemispheres begin receiving information from the ipsilateral visual field shortly after the initial peak, and that hemispheric asymmetries are not present in the first wave of ipsilateral information but only emerge afterward. The time course for integration, however, may be complex and variable across different ROIs.

The exceptional integration of visual information from both visual fields in right lateral fusiform gyrus may shed light on an interesting feature of acquired prosopagnosia. Face-selective areas are present in both the right and left hemisphere, but the great majority of prosopagnosia cases because of unilateral damage involve lesions to the right hemisphere. In fact, only five cases of unilateral left hemisphere damage have been reported (Barton, 2008; Wright, Wardlaw, Young, & Zeman, 2006; Mattson, Levin, & Grafman, 2000; Eimer & McCarthy, 1999; Tzavaras, Merienne, & Masure, 1973), four of whom were left-

handed (Bukowski, Dricot, Hanseeuw, & Rossion, 2013). Our findings suggest the differential effect of unilateral lesions on face recognition may be influenced by differences in how FFA in the right and left hemispheres integrate information. The rFFA appears to bring together face information from both visual fields, whereas the lFFA primarily processes face information in the LVF. Thus, when the rFFA is lesioned, face recognition is severely impaired. Although unilateral lesions to the lFFA may still impact face processing, this view suggests that the rFFA is still able to integrate and process face information across both visual fields and thus the loss of the lFFA has more limited effects on performance. If this account is correct, the rarity of both hemispatial neglect and acquired prosopagnosia cases because of left unilateral lesions arises, at least in part, from the greater integration of information from the ipsilateral visual field in the right hemisphere than the left hemisphere. This account also predicts that right unilateral lesions to FBA should result in greater impairments to body perception than left unilateral lesions. However, one case study of a right-handed patient with a unilateral lesion that included the rFBA suggests that the rFBA may not be as critical for body perception as the rFFA is for face perception (Susilo, Yang, Potter, Robbins, & Duchaine, 2015). Little is known though about FBA and its role in body perception, so it is possible that lFBA can compensate for the loss of rFBA. Given that this is only a single case, it is unclear whether the lFBA can compensate for the loss of the rFBA (unlike FFA) or whether bilateral lesions to FBA would be unlikely to produce behavioral deficits on body perception tasks. Further case studies of patients with lesions to the right, left, or bilateral FBA are needed to better understand the role that the FBA plays in integrating body information from across the visual field.

Reprint requests should be sent to Sarah B. Herald, Department of Psychological and Brain Sciences, Dartmouth College, 6207 Moore Hall, Hanover, N H 03755-3529, or via e-mail: sarahbherald@gmail.com.

Data Availability Statement

Stimuli, code, and anonymized data can be obtained by emailing the lead author. The original fMRI data cannot be shared because there is no IRB approval for sharing the data.

Author Contributions

Sarah B. Herald: Conceptualization; Data curation; Formal analysis; Investigation; Methodology; Visualization; Writing—Original draft; Writing—Review & editing. Hua Yang: Conceptualization; Formal analysis; Investigation; Methodology. Brad Duchaine: Conceptualization; Methodology; Project administration; Supervision; Writing—Review & editing.

Diversity in Citation Practices

Retrospective analysis of the citations in every article published in this journal from 2010 to 2021 reveals a persistent pattern of gender imbalance: Although the proportions of authorship teams (categorized by estimated gender identification of first author/last author) publishing in the *Journal of Cognitive Neuroscience* (*JoCN*) during this period were M(an)/M = .407, W(oman)/M = .32, M/W = .115, and W/W = .159, the comparable proportions for the articles that these authorship teams cited were M/M = .549, W/M = .257, M/W = .109, and W/W = .085 (Postle and Fulvio, *JoCN*, 34:1, pp. 1–3). Consequently, *JoCN* encourages all authors to consider gender balance explicitly when selecting which articles to cite and gives them the opportunity to report their article's gender citation balance.

REFERENCES

Argall, B. D., Saad, Z. S., & Beauchamp, M. S. (2006). Simplified intersubject averaging on the cortical surface using SUMA. *Human Brain Mapping*, *27*, 14–27. https://doi.org/10.1002/hbm.20158, PubMed: 16035046

Barton, J. J. S. (2008). Prosopagnosia associated with a left occipitotemporal lesion. *Neuropsychologia*, *46*, 2214–2224. https://doi.org/10.1016/j.neuropsychologia.2008.02.014, PubMed: 18374372

Brainard, D. H. (1997). The psychophysics toolbox. *Spatial Vision*, *10*, 433–436. https://doi.org/10.1163/156856897X00357, PubMed: 9176952

Bukowski, H., Dricot, L., Hanseeuw, B., & Rossion, B. (2013). Cerebral lateralization of face-sensitive areas in left-handers: Only the FFA does not get it right. *Cortex*, *49*, 2583–2589. https://doi.org/10.1016/j.cortex.2013.05.002, PubMed: 23906596

Chelazzi, L., Duncan, J., Miller, E. K., & Desimone, R. (1998). Responses of neurons in inferior temporal cortex during memory-guided visual search. *Journal of Neurophysiology*, *80*, 2918–2940. https://doi.org/10.1152/jn.1998.80.6.2918, PubMed: 9862896

Cox, R. W. (1996). AFNI: Software for analysis and visualization of functional magnetic resonance neuroimages. *Computers and Biomedical Research*, *29*, 162–173. https://doi.org/10.1006/cbmr.1996.0014, PubMed: 8812068

Cox, R. W., & Hyde, J. S. (1997). Software tools for analysis and visualization of fMRI data. *NMR in Biomedicine*, *10*, 171–178. https://doi.org/10.1002/(SICI)1099-1492(199706/08)10:4/5<171::AID-NBM453>3.0.CO;2-L, PubMed: 9430344

Dilks, D. D., Julian, J. B., Paunov, A. M., & Kanwisher, N. (2013). The occipital place area is causally and selectively involved in scene perception. *Journal of Neuroscience*, *33*, 1331–1336. https://doi.org/10.1523/JNEUROSCI.4081-12.2013, PubMed: 23345209

Downing, P. E., Jiang, Y., Shuman, M., & Kanwisher, N. (2001). A cortical area selective for visual processing of the human body. *Science*, *293*, 2470–2473. https://doi.org/10.1126/science.1063414, PubMed: 11577239

Driver, J., & Mattingley, J. B. (1998). Parietal neglect and visual awareness. *Nature Neuroscience*, *1*, 17–22. https://doi.org/10.1038/217, PubMed: 10195103

Driver, J., & Vuilleumier, P. (2001). Perceptual awareness and its loss in unilateral neglect and extinction. *Cognition*, *79*, 39–88. https://doi.org/10.1016/S0010-0277(00)00124-4, PubMed: 11164023

Dumoulin, S. O., & Wandell, B. A. (2008). Population receptive field estimates in human visual cortex. *Neuroimage*, *39*, 647–660. https://doi.org/10.1016/j.neuroimage.2007.09.034, PubMed: 17977024

Eimer, M., & McCarthy, R. A. (1999). Prosopagnosia and structural encoding of faces: Evidence from event-related potentials. *NeuroReport*, *10*, 255–259. https://doi.org/10.1097/00001756-199902050-00010, PubMed: 10203318

Finzi, D., Gomez, J., Nordt, M., Rezai, A. A., Poltoratski, S., & Grill-Spector, K. (2021). Differential spatial computations in ventral and lateral face-selective regions are scaffolded by structural connections. *Nature Communications*, *12*, 2278. https://doi.org/10.1038/s41467-021-22524-2, PubMed: 33859195

Fox, C. J., Iaria, G., & Barton, J. J. (2009). Defining the face processing network: Optimization of the functional localizer in fMRI. *Human Brain Mapping*, *30*, 1637–1651. https://doi.org/10.1002/hbm.20630, PubMed: 18661501

Gauthier, I., Tarr, M. J., Moylan, J., Skudlarski, P., Gore, J. C., & Anderson, A. W. (2000). The fusiform "face area" is part of a network that processes faces at the individual level. *Journal of Cognitive Neuroscience*, *12*, 495–504. https://doi.org/10.1162/089892900562165, PubMed: 10931774

Gomez, J., Natu, V., Jeska, B., Barnett, M., & Grill-Spector, K. (2018). Development differentially sculpts receptive fields across early and high-level human visual cortex. *Nature Communications*, *9*, 788. https://doi.org/10.1038/s41467-018-03166-3, PubMed: 29476135

Gross, C. G. (2008). Single neuron studies of inferior temporal cortex. *Neuropsychologia*, *46*, 841–852. https://doi.org/10.1016/j.neuropsychologia.2007.11.009, PubMed: 18155735

Heilman, K. M., & Van Den Abell, T. (1980). Right hemisphere dominance for attention: The mechanism underlying hemispheric asymmetries of inattention (neglect). *Neurology*, *30*, 327–330. https://doi.org/10.1212/WNL.30.3.327, PubMed: 7189037

Hemond, C. C., Kanwisher, N. G., & Op de Beeck, H. P. (2007). A preference for contralateral stimuli in human object- and face-selective cortex. *PLoS One*, *2*, e574. https://doi.org/10.1371/journal.pone.0000574, PubMed: 17593973

Husain, M., & Rorden, C. (2003). Non-spatially lateralized mechanisms in hemispatial neglect. *Nature Reviews Neuroscience*, *4*, 26–36. https://doi.org/10.1038/nrn1005, PubMed: 12511859

Ince, R. A. A., Jaworska, K., Gross, J., Panzeri, S., van Rijsbergen, N. J., Rousselet, G. A., et al. (2016). The deceptively simple N170 reflects network information processing mechanisms involving visual feature coding and transfer across hemispheres. *Cerebral Cortex*, *26*, 4123–4135. https://doi.org/10.1093/cercor/bhw196, PubMed: 27550865

Kay, K. N., Weiner, K. S., & Grill-Spector, K. (2015). Attention reduces spatial uncertainty in human ventral temporal cortex. *Current Biology*, *25*, 595–600. https://doi.org/10.1016/j.cub.2014.12.050, PubMed: 25702580

Kleiner, M., Brainard, D., & Pelli, D. (2007). What's new in Psychtoolbox-3? *Perception*, *36*, 1–16.

Li, X., Morgan, P. S., Ashburner, J., Smith, J., & Rorden, C. (2016). The first step for neuroimaging data analysis: DICOM to NIfTI conversion. *Journal of Neuroscience Methods*, *264*, 47–56. https://doi.org/10.1016/j.jneumeth.2016.03.001, PubMed: 26945974

Mattson, A. J., Levin, H. S., & Grafman, J. (2000). A case of prosopagnosia following moderate closed head injury with left hemisphere focal lesion. *Cortex*, *36*, 125–137. https://doi.org/10.1016/S0010-9452(08)70841-4, PubMed: 10728902

Nachev, P., & Husain, M. (2006). Disorders of visual attention and the posterior parietal cortex. *Cortex*, *42*, 766–773. https://doi.org/10.1016/S0010-9452(08)70415-5, PubMed: 16909637

Peelen, M. V., & Downing, P. E. (2005). Selectivity for the human body in the fusiform gyrus. *Journal of Neurophysiology 93*, 603–608. https://doi.org/10.1152/jn.00513.2004, PubMed: 15295012

Pelli, D. G. (1997). The VideoToolbox software for visual psychophysics: Transforming numbers into movies. *Spatial Vision*, *10*, 437–442. https://doi.org/10.1163/156856897X00366, PubMed: 9176953

Pitcher, D., Dilks, D. D., Saxe, R. R., Triantafyllou, C., & Kanwisher, N. (2011). Differential selectivity for dynamic versus static information in face-selective cortical regions. *Neuroimage*, *56*, 2356–2363. https://doi.org/10.1016/j.neuroimage.2011.03.067, PubMed: 21473921

Pitcher, D., Pilkington, A., Rauth, L., Baker, C., Kravitz, D. J., & Ungerleider, L. G. (2020). The human posterior superior temporal sulcus samples visual space differently from other face-selective regions. *Cerebral Cortex*, *30*, 778–785. https://doi.org/10.1093/cercor/bhz125, PubMed: 31264693

Pitcher, D., & Ungerleider, L. G. (2021). Evidence for a third visual pathway specialized for social perception. *Trends in Cognitive Sciences*, *25*, 100–110. https://doi.org/10.1016/j.tics.2020.11.006, PubMed: 33334693

Rauschecker, A. M., Bowen, R. F., Parvizi, J., & Wandell, B. A. (2012). Position sensitivity in the visual word form area. *Proceedings of the National Academy of Sciences, U.S.A.*, *109*, E1568–E1577. https://doi.org/10.1073/pnas.1121304109, PubMed: 22570498

Reddy, L., Kanwisher, N. G., & VanRullen, R. (2009). Attention and biased competition in multi-voxel object representations. *Proceedings of the National Academy of Sciences, U.S.A.*, *106*, 21447–21452. https://doi.org/10.1073/pnas.0907330106, PubMed: 19955434

Rosenke, M., Weiner, K. S., Barnett, M. A., Zilles, K., Amunts, K., Goebel, R., et al. (2018). A cross-validated cytoarchitectonic atlas of the human ventral visual stream. *Neuroimage*, *170*, 257–270. https://doi.org/10.1016/j.neuroimage.2017.02.040, PubMed: 28213120

Saad, Z. S., & Reynolds, R. C. (2012). SUMA. *Neuroimage*, *62*, 768–773. https://doi.org/10.1016/j.neuroimage.2011.09.016, PubMed: 21945692

Saad, Z. S., Reynolds, R. C., Argall, B., Japee, S., & Cox, R. W. (2004). SUMA: An interface for surface-based intra-and inter-subject analysis with AFNI. In *2004 2nd IEEE international symposium on biomedical imaging: Nano to macro (IEEE cat no. 04EX821)* (pp. 1510–1513). IEEE. https://doi.org/10.1109/ISBI.2004.1398837

Sayres, R., & Grill-Spector, K. (2008). Relating retinotopic and object-selective responses in human lateral occipital cortex. *Journal of Neurophysiology*, *100*, 249–267. https://doi.org/10.1152/jn.01383.2007, PubMed: 18463186

Setsompop, K., Gagoski, B. A., Polimeni, J. R., Witzel, T., Wedeen, V. J., & Wald, L. L. (2012). Blipped-controlled aliasing in parallel imaging for simultaneous multislice echo planar imaging with reduced G-factor penalty. *Magnetic Resonance in Medicine*, *67*, 1210–1224. https://doi.org/10.1002/mrm.23097, PubMed: 21858868

Silson, E. H., Chan, A. W.-Y., Reynolds, R. C., Kravitz, D. J., & Baker, C. I. (2015). A Retinotopic basis for the division of high-level scene processing between lateral and ventral human occipitotemporal cortex. *Journal of Neuroscience*,

35, 11921–11935. https://doi.org/10.1523/JNEUROSCI.0137 -15.2015, PubMed: 26311774

Silson, E. H., Groen, I. I. A., Kravitz, D. J., & Baker, C. I. (2016). Evaluating the correspondence between face-, scene-, and object-selectivity and retinotopic organization within lateral occipitotemporal cortex. *Journal of Vision*, *16*, 14. https://doi .org/10.1167/16.6.14, PubMed: 27105060

Silson, E. H., Groen, I. I., & Baker, C. I. (2022). Direct comparison of contralateral bias and face/scene selectivity in human occipitotemporal cortex. *Brain Structure and Function*, *227*, 1405–1421. https://doi.org/10.1007/s00429 -021-02411-8, PubMed: 34727232

Susilo, T., Yang, H., Potter, Z., Robbins, R., & Duchaine, B. (2015). Normal body perception despite the loss of right fusiform gyrus. *Journal of Cognitive Neuroscience*, *27*, 614–622. https://doi.org/10.1162/jocn_a_00743, PubMed: 25313655

Taylor, P. A., Chen, G., Glen, D. R., Rajendra, J. K., Reynolds, R. C., & Cox, R. W. (2018). FMRI processing with AFNI: Some comments and corrections on "exploring the impact of analysis software on task fMRI results". *bioRxiv*. https://doi .org/10.1101/308643

Towler, J., & Eimer, M. (2015). Early stages of perceptual face processing are confined to the contralateral hemisphere: Evidence from the N170 component. *Cortex*, *64*, 89–101. https://doi.org/10.1016/j.cortex.2014.09.013, PubMed: 25461710

Tzavaras, A., Merienne, L., & Masure, M. C. (1973). Facial agnosia, amnesia and disorders of speech due to left temporal injury in a left handed subject. *Encephale*, *62*, 382–394, PubMed: 4794621

Uyar, F., Shomstein, S., Greenberg, A. S., & Behrmann, M. (2016). Retinotopic information interacts with category selectivity in human ventral cortex. *Neuropsychologia*, *92*, 90–106. https://doi.org/10.1016/j.neuropsychologia.2016.05 .022, PubMed: 27241486

Weiner, K. S. (2019). The mid-fusiform sulcus (sulcus sagittalis gyri fusiformis). *Anatomical Record*, *302*, 1491–1503. https:// doi.org/10.1002/ar.24041, PubMed: 30471211

Weiner, K. S., Golarai, G., Caspers, J., Chuapoco, M. R., Mohlberg, H., Zilles, K., et al. (2014). The mid-fusiform sulcus: A landmark identifying both cytoarchitectonic and functional divisions of human ventral temporal cortex. *Neuroimage*, *84*, 453–465. https://doi.org/10.1016/j.neuroimage.2013.08.068, PubMed: 24021838

Wickham, H., Averick, M., Bryan, J., Chang, W., McGowan, L., François, R., et al. (2019). Welcome to the Tidyverse. *Journal of Open Source Software*, *4*, 1686. https://doi.org/10.21105 /joss.01686

Wright, H., Wardlaw, J., Young, A. W., & Zeman, A. (2006). Prosopagnosia following nonconvulsive status epilepticus associated with a left fusiform gyrus malformation. *Epilepsy & Behavior*, *9*, 197–203. https://doi.org/10.1016/j.yebeh.2006.04 .010, PubMed: 16777488